

Atmospheric neutrino oscillation analysis with sub-leading effects in Super-Kamiokande I,II

SK Collaboration
(Dated: February 17, 2009)

We present a search for non-zero θ_{13} and deviations of $\sin^2\theta_{23}$ from 0.5 in the oscillations of atmospheric neutrino data of the Super-Kamiokande I and Super-Kamiokande II. No distortions of the neutrino flux consistent with positive θ_{13} are found and both neutrino mass hierarchy hypotheses are in agreement with the data. The data are best fit at $\Delta m^2 = 2.1 \times 10^{-3} \text{eV}^2$, $\sin^2\theta_{13} = 0.0$ and $\sin^2\theta_{23} = 0.5$. In the normal (inverted) hierarchy is found at the 90% confidence level. The atmospheric mixing angle is within, $0.43 \leq \sin^2\theta_{23} \leq 0.55$ at the 1-sigma C.L.. In the normal (inverted) hierarchy θ_{13} is constrained $\sin^2\theta_{13} < 0.07(0.13)$.

PACS numbers: some numbers here

I. INTRODUCTION

Despite several experimental measurements [1–8] constraining neutrino flavor oscillations, the nature of the neutrino mass hierarchy and whether or not θ_{13} is non-zero remain open questions. The latter is the last unknown mixing angle and is currently the subject of a research program including beam and reactor based experiments [9–11]. At present the CHOOZ [12] experiment provides the best upper limit on the size of θ_{13} , but a non-zero value may manifest itself and be observable in the event rate of multi-GeV electron neutrinos passing through the earth. Similarly, though atmospheric neutrino data is well fit to “maximal atmospheric mixing” with $\theta_{23} = \pi/4$, $\nu_\mu \leftrightarrow \nu_e$ transitions driven by solar oscillation parameters appear at sub-GeV energies when the atmospheric mixing deviates from this value. The questions of whether or not θ_{23} is exactly $\pi/4$, the nature of θ_{13} and the sign of the neutrino mass hierarchy all contribute to an eight-fold degeneracy [13] of oscillation parameter solutions when considering CP-Violation in neutrinos. For future experimental searches of CP-Violation, answers to these questions are essential.

In this paper two analyses are presented searching for evidence of sub-leading oscillation effects which address these questions and appear as changes in the ν_e flux of the atmospheric neutrino samples at Super-Kamiokande (Super-K,SK). The first is an improved extension of a three flavor oscillation analysis performed using the first phase of the experiment (SK-I) [2]. An updated analysis using both the first and second (SK-II) phases is presented. Both data sets are then used in the second analysis to test whether $\sin^2\theta_{23}$ is non-maximal.

II. SUB-DOMINANT EFFECTS IN ATMOSPHERIC NEUTRINO OSCILLATIONS

Neutrino oscillations in three flavors are parameterized by six parameters: Two mass squared differences, Δm_{12}^2 , Δm_{13}^2 , where $\Delta m_{ij}^2 = m_j^2 - m_i^2$, a CP violating parameter δ_{CP} , and three mixing angles θ_{ij} , ($i \neq j$). Each mixing angle parameterizes a rotation, U_{ij} , between pairs mass states inside of the three-dimensional oscillation space. The correspondence between neutrino mass eigenstates and their flavor eigenstates is then,

$$|\nu_\alpha\rangle = \sum_i^3 U_{\alpha,i}^* |\nu_i\rangle, \quad (1)$$

where U is the 3×3 matrix defined by $U_{23}U_{13}U_{12}$. Non-zero mixing angles and non-degenerate mass eigenvalues give rise to standard neutrino oscillations, where the amplitude of oscillations is proportional to $\sin^2\theta$ and its frequency is proportional two Δm^2 . Observations of solar[3, 5] and reactor [1] neutrinos are well described by oscillations governed by the “1-2” (solar) parameters while those of atmospheric [4] and accelerator neutrinos are described by the “2-3” (atmospheric) parameters. These measurements have established two oscillation regimes whose frequencies differ by two orders of magnitude. The third set of parameters has been probed by CHOOZ, a reactor neutrino disappearance experiment sensitive to oscillations at the atmospheric Δm^2 , which placed a limit on mixing in this channel at $\sin^2\theta_{13} < 0.04$ for $\Delta m^2 \sim 2.0 \times 10^{-3} \text{eV}^2$ at 90% confidence[12].

For the purposes of studying sub-dominant oscillations in atmospheric neutrinos it is useful to separate the discussion of oscillation probabilities into two domains, $\theta_{13} \sim 0$ such that $U_{13} \sim \mathbf{I}$ and otherwise. The observable effects each domain has on the atmospheric neutrino sample can similarly be divided into two energy regimes and motivates two separate analyses with distinct focii: each analysis has been tailored to search its regime of interest.

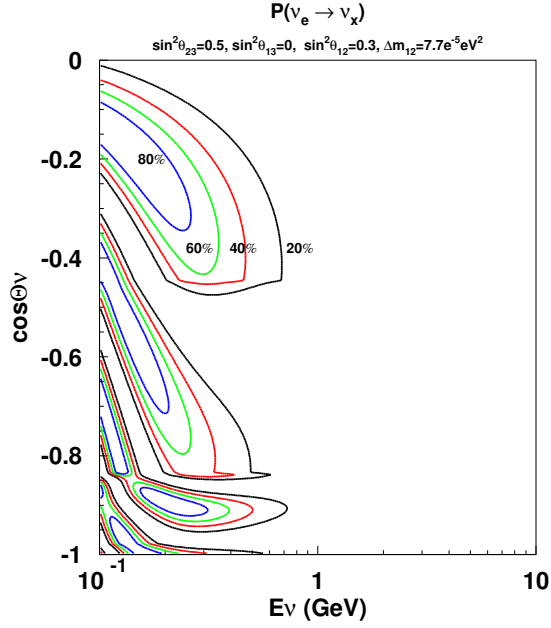


FIG. 1: The calculated ν_e transition probability P_2 for atmospheric neutrinos with an energy E_ν (horizontal axis) and a direction of $\cos\Theta_\nu$ (vertical axis). The 1-2 oscillation parameters are assumed to be $\Delta m_{12}^2 = 7.7 \times 10^{-5} eV^2$ and $\sin^2\theta_{12} = 0.30$. The Earth's matter effect is taken into account.

If the transition probability ($\nu_e \rightarrow \nu_\mu$) in matter driven by $\sin^2\theta_{12}$, Δm_{12}^2 (solar terms) is denoted as P_2 , and assuming $\theta_{13} = 0$, the oscillation probabilities of ν_e and ν_μ are [14, 15]:

$$P(\nu_e \rightarrow \nu_e) = 1 - P_2, \quad (2)$$

$$P(\nu_e \rightarrow \nu_\mu) = P(\nu_\mu \rightarrow \nu_e) = c_{23}^2 P_2, \quad (3)$$

$$P(\nu_\mu \rightarrow \nu_\mu) = 1 - c_{23}^4 P_2 - 2s_{23}^2 c_{23}^2 \left(1 - \sqrt{1 - P_2 \cos \phi}\right), \quad (4)$$

$$\phi \sim \left(\Delta m_{31}^2 + s_{12}^2 \Delta m_{21}^2\right) \frac{L}{2E_\nu}. \quad (5)$$

Therefore, the oscillated atmospheric electron and muon neutrino fluxes are expressed by :

$$\begin{aligned} F_e^{osc} &= F_e^0 \cdot P(\nu_e \rightarrow \nu_e) + F_\mu^0 \cdot P(\nu_\mu \rightarrow \nu_e) \\ &= F_e^0 (1 + P_2(r c_{23}^2 - 1)), \end{aligned} \quad (6)$$

$$\begin{aligned} F_\mu^{osc} &= F_e^0 \cdot P(\nu_e \rightarrow \nu_\mu) + F_\mu^0 \cdot P(\nu_\mu \rightarrow \nu_\mu) \\ &= F_\mu^0 \left(1 - \frac{c_{23}^2}{r} (r c_{23}^2 - 1) P_2 - \frac{1}{2} \sin^2 2\theta_{23} (1 - \sqrt{1 - P_2 \cos \phi})\right), \end{aligned} \quad (7)$$

where F_e^0 and F_μ^0 are the atmospheric neutrino fluxes without oscillations. r is the ratio of the original muon and electron neutrino fluxes F_μ^0/F_e^0 , which is ~ 2 for neutrinos in the low energy region.

Figure 1 shows the calculated P_2 for atmospheric neutrinos with an energy E_ν and a direction Θ_ν assuming $\Delta m_{12}^2 = 7.7 \times 10^{-5} eV^2$ and $\sin^2\theta_{12} = 0.30$. Since the oscillation effect is larger in the lower energy region as shown in Figure 1, the Sub-GeV atmospheric neutrino events play an important role to observe the sub-dominant oscillation effect.

The atmospheric electron neutrino flux decreases by P_2 , at the same time, it increases by the muon neutrino oscillation (Equation (3)). The atmospheric electron neutrino flux changes by the effect of oscillations driven by the 1-2 parameters and the size of the oscillation effect depends on $\cos^2\theta_{23}$ as seen in Equation (6). Equation (6) can be rewritten as follows :

$$\frac{F_e^{osc}}{F_e^0} - 1 = P_2(r \cos^2 \theta_{23} - 1). \quad (8)$$

Since the flavor ratio r is approximately 2 in the Sub-GeV neutrino energy region, in the case of $\cos^2 \theta_{23} = 0.5$ (i.e. $\sin^2 \theta_{23} = 0.5$, $\theta_{23} = 45^\circ$), the increasing and decreasing effects on the electron neutrino flux are expected to be canceled out. If $\cos^2 \theta_{23} > 0.5$ (i.e. $\sin^2 \theta_{23} < 0.5$, $\theta_{23} < 45^\circ$), an excess of the Sub-GeV e-like sample is expected. If $\cos^2 \theta_{23} < 0.5$ (i.e. $\sin^2 \theta_{23} > 0.5$, $\theta_{23} > 45^\circ$), the Sub-GeV e-like sample is expected to be reduced. Therefore it may be possible to determine the octant of θ_{12} by searching for changes in the flux of the sub-GeV electron-like samples at SK. The change in the low energy ν_e flux is shown in figure 2. At higher neutrino energies $r > 3$ so the effect of $\cos^2 \theta_{23}$ is diminished.

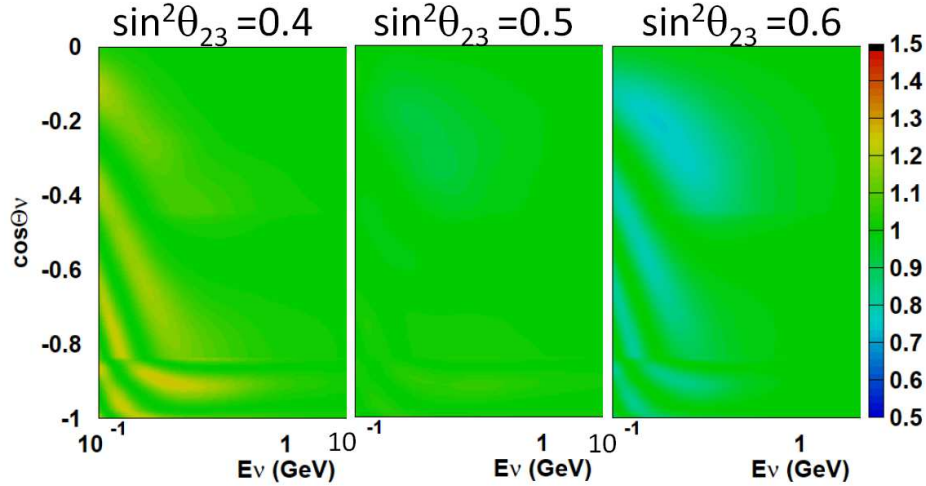


FIG. 2: The electron neutrino flux ratio as a function of neutrino zenith angle and energy for oscillations including the solar parameters and $\theta_{23} \neq \pi/4$ relative to oscillations at $\theta_{23} = \pi/4$. Negative $\cos \Theta_\nu$ corresponds to upward-going neutrinos and 0 is the horizon. An expected deficit (excess) for atmospheric mixing in the first (second) octant is shown at left (right). The island shapes are regions of probability driven by the solar oscillation parameters.

When θ_{13} is non-zero the matrix U_{13} is no longer sufficiently close to unity, and the above relations do not hold. Instead in the search for non-zero θ_{13} the oscillation analysis is done using a “one mass scale dominant” scheme wherein the solar neutrino mass difference is taken to be much smaller than the atmospheric mass difference. Accordingly, the solar mass difference is neglected and a single mass splitting is adopted, $\Delta m^2 \equiv |m_3^2 - m_{1,2}^2|$ such that $\Delta m^2 > (<)0$ corresponds to the normal (inverted) mass hierarchy. Under this framework the three-neutrino oscillation probability in constant density matter may be written [16] as

$$P(\nu_\mu \leftrightarrow \nu_e) = \sin^2 \theta_{23} \sin^2 2\theta_{13}^M \sin^2 \left(\frac{1.27 \Delta m_M^2 L}{E} \right) \quad (9)$$

Here L and E are the neutrino propagation length and energy, respectively. The matter modified mixing parameters are

$$\begin{aligned} \Delta m_M^2 &= \Delta m^2 \sqrt{\sin^2 2\theta_{13} + (\Gamma - \cos 2\theta_{13})^2} \\ \sin^2 2\theta_{13}^M &= \frac{\sin^2 2\theta_{13}}{\sin^2 2\theta_{13} + (\Gamma - \cos 2\theta_{13})^2}, \end{aligned} \quad (10)$$

where $\Gamma = \pm 2\sqrt{2}G_f n_e E / \Delta m^2$, G_f is the Fermi constant, n_e is the local electron density and the top (bottom) of double sign specifies neutrinos (anti neutrinos). Resonant enhancement of the oscillation probability occurs when $\Gamma = \cos \theta_{13}$ and occurs for either neutrinos or anti-neutrinos depending on the mass hierarchy. Further, when θ_{13} is 0 there is no enhancement.

Oscillation probabilities for neutrinos traversing the earth appear in figure 3. For $\Delta m^2 \sim 2 \times 10^{-3} \text{eV}^2$ this resonance occurs in the 3-10 GeV region and its strength increases with θ_{13} reaching $\sim 40\%$ conversion probability near the CHOOZ limit. Under these conditions the primary signature in the atmospheric neutrino sample at Super-K is an increased rate of high energy upward-going electron-like events. Additional effects on muon event rates are expected, but are generally much smaller. For large values of θ_{13} an expected $\sim 20\%$ increase in the multi-Ring electron-like event rate would be accompanied by a $\sim 5\%$ change in similarly energetic muon-like samples.

Oscillation probabilities in both analyses are computed using a numerical technique based on ref. [17]. Probabilities inside the Earth are computed using a piecewise constant radial matter density profile constructed as the median density in each of the dominant regions of the PREM [18] model: inner core ($0 \leq r < 1220\text{km}$) 13.0 g/cm^3 , outer core ($1220 \leq r < 3480\text{km}$) 11.3 g/cm^3 , mantle ($3480 \leq r < 5701\text{km}$) 5.0 g/cm^3 and the crust ($5701 \leq r < 6371\text{km}$) 3.3 g/cm^3 . The difference in the oscillation probabilities using this model compared to the more expansive one after incorporating detector resolution effects have a negligible impact on the final analysis results.

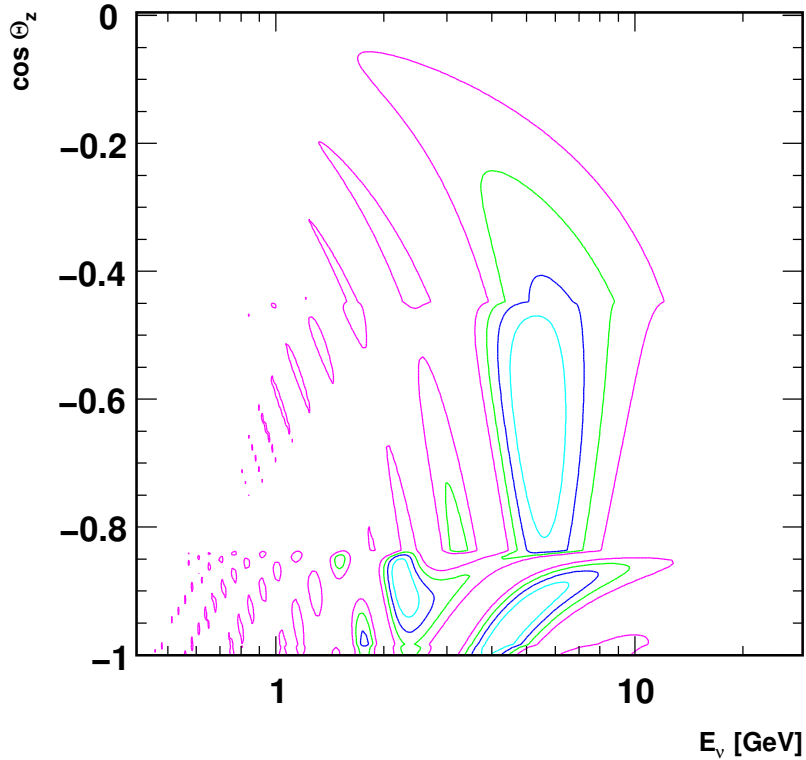


FIG. 3: Three-flavor oscillation probability $\nu_\mu \leftrightarrow \nu_e$ for θ_{13} at the CHOOZ limit for neutrinos under the normal hierarchy in the one mass scale dominant framework. A matter induced resonant between 3-10 GeV appears for upward going neutrinos that traverse the inner and out regions of the Earth's core. Atmospheric mixing is included at $(\Delta m_{23}^2, \sin^2 \theta_{23}) = (2.1 \times 10^{-3} \text{ eV}^2, 0.5)$.

III. DATA SAMPLE

Super-Kamiokande is a cylindrical 50 kton water Cerenkov detector situated at a depth of 2700 meters water equivalent. The detector volume is optically separated into an inner volume (ID) and an outer veto region (OD). During the SK-I (SK-II) period the ID was instrumented with 11,146 (5,182) inward facing 20-inch photomultiplier tubes (PMTs) and the OD with 1,885 outward facing 8-inch PMTs. In SK-II, the ID PMTs have been encased in fiber-reinforced acrylic shells to prevent chain reactions within the detector in the event of a PMT implosion. A more detailed description of the detector may be found in [19].

In this paper, atmospheric neutrino events are organized into three classes, fully contained (FC), partially contained (PC) and upward-going muons (UP μ). Events which deposit all of their Cerenkov light in the ID are classified as FC, while events that originate in the ID but have an exiting particle depositing energy in the OD are considered PC. Neutrino interactions occurring in the rock beneath the detector which produce muons that traverse (through-going) or stop in the detector (stopping) are classified as UP μ events. Data accrued in the five years spanning the SK-I run

		FC Sub-GeV single-ring e-like			
		0 μ edecay	1 μ edecay	π^0 -like	all
number of events (MC)		????(?? %)	????(?? %)	????(?? %)	????(100. %)
CC $\nu_e + \bar{\nu}_e$	Q.E.	80.4 %	2.2 %	17.2 %	71.3 %
	single meson	12.2 %	56.1 %	9.1 %	14.9 %
	multi π	1.5 %	14.6 %	3.3 %	2.5 %
	coherent π	0.1 %	0.7 %	0.07 %	0.2 %
CC $\nu_\mu + \bar{\nu}_\mu$		0.7 %	17.7 %	10.0 %	2.4 %
NC		4.9 %	8.9 %	59.9 %	8.7 %

		FC Sub-GeV single-ring μ -like			
		0 μ edecay	1 μ edecay	2 μ edecay	all
number of events (MC)		????(?? %)	????(?? %)	????(?? %)	????(100. %)
CC $\nu_\mu + \bar{\nu}_\mu$	Q.E.	72.9 %	79.3 %	2.9 %	74.4 %
	single meson	13.0 %	15.9 %	71.5 %	17.0 %
	multi π	1.4 %	2.1 %	21.1 %	2.6 %
	coherent π	0.1 %	0.2 %	0.7 %	0.2 %
CC $\nu_e + \bar{\nu}_e$		1.5 %	0.07 %	0.05 %	0.5 %
NC		10.9 %	2.3 %	2.2 %	5.1 %

TABLE I: Fraction of each neutrino interaction mode in FC Sub-GeV atmospheric neutrino Monte Carlo events.

period starting in 1996 correspond to 1489 live-days of FC and PC events with 1646 UP μ live-days. SK-II data was taken between December 2002 and October 2005 and represents 799 live-days of FC and PC events and 828 live-days of UP μ events. The difference of livetimes between FC/PC and UP μ is due to the insensitivity of the UP μ reduction to noise such as “flasher” PMTs. Such noise may be misconstrued as real events in the FC/PC reductions so data surrounding these events is rejected.

Fully contained events are further divided into sub-GeV and multi-GeV subsamples based on the events visible energy, E_{vis} . Events with $E_{\text{vis}} < 1.33$ GeV are sub-GeV. The number of reconstructed Cerenkov rings in an event is also used to separate these samples into single- and multi-ring subsamples. Single-ring events are classified into μ -like and e-like samples by the ring pattern. For multi-ring sample, the most energetic ring is used to identify the particle type. Partially contained events are classified as “OD stopping” or “OD through-going” based on their energy deposition in the OD [20]. Similarly UP μ events that traverse the detector are separated into “showering” and “non-showering” based on the method in ref. [21] while those that enter and stop within the detector are classified as “stopping.” These samples are made for both SK-I and SK-II and are separate throughout the analysis.

To increase the purity of the interaction mode in each sample, FC Sub-GeV single-ring events are separated into more finer samples by using the information such as the number of decay electrons. The FC Sub-GeV single-ring e-like sample contains events which are mainly π^0 events from $\nu N \rightarrow \nu N \pi^0$ interactions and can be background. These π^0 events are separated from ν_e -enriched samples using the likelihood analysis. After the separation of π^0 -like sample, the rest of e-like events are separated to two categories, 0 μ edecay which has no decay electron and 1 μ edecay which has one or more decay electrons. The CCQE fraction of 0 μ edecay sample is improved and NC events is decreased (Table I). For the FC Sub-GeV single-ring μ -like sample, there are three categories using the number of decay electrons as 0 μ edecay, 1 μ edecay and 2 μ edecay, corresponding no decay electron, 1 decay electron and 2 or more decay electrons sample. 1 μ edecay sample can increase the CCQE fraction and decrease the NC fraction. Detail improvements from these categorizing are shown in Table I. Since these improvements are useful to look for the excess of ν_e in the low energy region by the sub-dominant effect due to the solar neutrino parameters, the finer separated samples can make good sensitivity to search for non-maximal $\sin^2\theta_{23}$.

To improve the analysis’ sensitivity to ν_e appearance induced by non-zero θ_{13} , an enhanced FC multi-GeV multi-Ring electron-like sample is created. The selection is based on the likelihood method as described in ref. [2] for SK-I and is extended in this analysis to SK-II. The likelihood functions have been built using 500 years of MC incorporating recent improvements to the SK reconstruction algorithms. Accordingly, the event populations of the SK-I sample here differ from that in the reference.

The MC is divided into five energy bins, 1.33-2.5 GeV, 2.5-5 GeV, 5-10 GeV, 10-20 GeV and > 20 GeV and PDFs for each bin are constructed using events whose most energetic ring has been reconstructed as electron-like. Four observables are used in the event selection: the number of decay electrons in the event, the maximum distance between

TABLE II: The expected number of events for each interaction component of the multi-ring multi-GeV e-like sample after likelihood selection for the SK-I and SK-II MC scaled to 1489.2 and 798.6 livetime days respectively. Two-flavor neutrino oscillations $\nu_\mu \leftrightarrow \nu_\tau$ have been applied at $\Delta m^2 = 2.1 \times 10^{-3} \text{ eV}^2$ and $\sin^2 2\theta = 1.0$.

	CC $\nu_e + \bar{\nu}_e$	CC $\nu_\mu + \bar{\nu}_\mu$	NC	Total
SK-I	331.0	39.2	74.4	444.6
Percentage (%)	74.5	8.8	16.7	100.0
SK-II	178.0	23.4	42.8	244.2
Percentage (%)	72.9	9.6	17.5	100.0

the neutrino vertex and any muon decay electrons, the fraction of momentum carried by the event's most energetic ring and its PID likelihood value. The final likelihood functions are defined as,

$$\mathcal{L}_j = \sum_{i=1}^4 \log(\Gamma_i^S(x_i)) - \log(\Gamma_i^B(x_i)), \quad (11)$$

where Γ_i represents the PDF for the i^{th} observable and x_i is the observables measured value. The superscripts S and B label the signal and background PDFs respectively. In selecting electron neutrino events, the signal is taken to be CC $\nu_e + \bar{\nu}_e$, while the background is composed of CC $\nu_\mu + \bar{\nu}_\mu$ and NC events. An event makes it into the final sample if it passes all cuts in the FC reduction, if the event's most energetic ring is electron-like, and if $\mathcal{L}_j > 0$. Table II shows the event compositions of the multi-GeV e-like sample after this selection for SK-I and SK-II.

The summary of all atmospheric neutrino events for DATA and Monte Carlo events show Table.III. (– NOT COLLECTED YET)

IV. OSCILLATION ANALYSIS

An oscillation analysis has been performed using the above data samples to search for evidence of non-zero θ_{13} . Since the physical detector configuration differs between SK-I and SK-II, separate 500 years equivalent MC data sets for each run period are used. The data are compared against the MC expectation using a ‘‘pulled’’ χ^2 method based a Poisson probability distribution:

$$\chi^2 = 2 \sum_n \left(E_n(1 + \sum_i f_n^i \epsilon_i) - \mathcal{O}_n + \mathcal{O}_n \ln \frac{\mathcal{O}_n}{E_n(1 + \sum_i f_n^i \epsilon_i)} \right) + \sum_i \left(\frac{\epsilon_i}{\sigma_i} \right)^2, \quad (12)$$

where n indexes the data bins, E_n is the MC expectation and \mathcal{O}_n is the number of observed events in the n^{th} bin. Systematic errors are incorporated into the fit via the systematic error parameter ϵ_i , where i is the systematic error index, f_n^i is the fractional change in the MC expectation in bin n for a 1-sigma change in the i^{th} systematic error. The 1-sigma value of a systematic error is labeled as σ_i .

To ensure stability of the function in equation 12 the binning has been chosen so that there are at least 6 expected MC events in each bin after scaling to the appropriate livetime. Data are binned separately between SK-I and SK-II, with a total of 400 bins in former and 350 in the latter. In SK-I and SK-II the decay electron samples are divided into 5 momentum and 10 zenith angle bins for the e-like 0, μ -like 0 and μ -like 1 samples and 1 zenith bin otherwise. Other SK-I (SK-II) FC events are divided into 14 (10) momentum bins, PC events into 6 (4) bins and all UP μ samples have one momentum bin each. All of these samples are further divided into 10 evenly spaced zenith angle bins. FC and PC events range from $-1 \leq \cos\Theta \leq 1$ and UP μ events are binned from $-1 \leq \cos\Theta \leq 0$.

Systematics in the analysis are separated into detector and reconstruction systematics which differ between SK-I and SK-II and flux or interaction cross section dependent systematics that are common between the two. There are 90 sources of uncertainty in total, 26 of which are common and 37 independent errors for each of SK-I and SK- II. The effect of the systematic errors are introduced by the error coefficients f_n^i which are computed for every bin and error in the analysis.

	SK-I		SK-II	
	Data	Monte Carlo	Data	Monte Carlo
FC Sub-GeV				
single-ring				
<i>e</i> -like	3353	2789.2	1842	1494.8
0 μ edecay	2930	2434.8	1607	1302.1
1 μ edecay	259	179.1	147	103.4
π^0 -like	164	175.2	91	89.3
μ -like	3227	4132.7	1718	2155.3
0 μ edecay	1028	1338.6	576	727.5
1 μ edecay	2049	2644.4	1059	1347.9
2 μ edecay	150	149.7	83	79.8
2-ring π^0 -like	506	379.3	266	203.2
FC Multi-GeV				
single-ring				
<i>e</i> -like	746	667.7	417	415.7
μ -like	651	881.3	379	496.2
multi-ring				
μ -like	647	1017.4	349	504.6
PC	911	1143.8	427	588.4
Upward-going muon				
stopping	417.7	721.4	208.6	338.3
non-showering	1544.8	1429.1	771.2	741.9
showering	296.5	251.0	105.4	89.9

TABLE III: Summary of atmospheric neutrino events for data and Monte Carlo events of FC, PC and upward-going muon samples for SK-I and SK-II. The live time of FC and PC is 1489.2 days for SK-I and 798.6 days for SK-II and the live time of upward-going muon samples is 1645.9 days for SK-I and 827.7 days for SK-II. The number of the Monte Carlo events is normalized by the live time of the data.

A. Search for θ_{13}

In the search for θ_{13} oscillation fits are performed by scanning a grid of 83,025 oscillation points in three variables, $\log_{10}\Delta m^2$, $\sin^2\theta_{23}$ and $\sin^2\theta_{13}$. Equation 12 is minimized with respect to the ϵ_i at each of these points according to $\frac{\partial\chi^2}{\partial\epsilon_i} = 0$. This derivative yields a set of linear equations[22] in ϵ that can be solved iteratively. The best fit point is defined as the global minimum χ^2 on the grid of oscillation points.

The fitting procedure has been performed on the SK-I, SK-II and SK-I+SK-II data sets assuming both a normal and inverted hierarchy. The results are summarized in table IV. For SK-I+SK-II, the SK-I and SK-II bins are considered simultaneously but remain separate during the fit. In the both hierarchies the best fit point in SK-I + SK-II is at $(\Delta m^2, \sin^2\theta_{13}, \sin^2\theta_{23}) = (2.1 \times 10^{-3}\text{eV}^2, 0.0, 0.5)$ with $\chi^2_{\min} = 841.7$ for 745 DOF. Therefore, there is no preference in the data for either mass hierarchy. Allowed regions at 90%(99%) are drawn in two dimensions at $\chi^2 = \chi^2_{\min} + 4.6(9.2)$. The third parameter in these projections has been minimized over. Computing the 90% critical value using a Feldman-Cousins type procedure confirmed that 4.6 (9.0) is the correct value in this scheme. The resulting allowed regions are shown in figures 4 and 5.

Figure 6 shows the Δm^2 vs. θ_{13} plane for each of the fits in the normal hierarchy overlaid with the CHOOZ [12] 90% C.L. exclusion contour. All of the fits are in agreement with the CHOOZ result. However, despite having only slightly more than half of the livetime of SK-I, the constraint on the size of the $\sin^2\theta_{13}$ contour is more severe in SK-II. In the SK-II data, this constraint comes from a downward fluctuation relative to the MC expectation in two of the steepest upward going zenith angle bins of the multi-GeV single-ring *e*-like sample. For non-zero values of θ_{13} , the increased conversion probability from $\nu_\mu \leftrightarrow \nu_e$ tends to populate these bins with more events. Therefore, the disparity between data and MC is increasingly exacerbated for larger values of the parameter. Similarly, there is an upward going fluctuation in the $\cos\Theta_z = -0.6$ bin of the upward-stopping μ sample where non-zero θ_{13} suppresses the event rate in this bin. The SK-I data does not have these kinds of fluctuations so when fit together with SK-II, the

TABLE IV: Best Fit information for for the six fits done in the search for θ_{13} . In the SK-I+SK-II fits both the normal and inverted hierarchies have the same best fit point, indicating no preference for either in the data.

	$\sin^2\theta_{13}$ 90% C.L.	$\sin^2\theta_{13}$	Δm^2	$\sin^2\theta_{23}$	$\chi^2/\text{D.O.F}$
Normal Hierarchy					
SK-I	< 0.13	0.01	2.2	0.52	429.4 / 397
SK-II	< 0.10	0.00	2.6	0.50	413.1 / 347
SK-I+II	< 0.07	0.00	2.1	0.50	841.7 / 745
Inverted Hierarchy					
SK-I	< 0.25	0.04	2.2	0.55	429.9 / 397
SK-II	< 0.16	0.00	2.6	0.50	413.1 / 347
SK-I+II	< 0.13	0.00	2.1	0.50	841.7 / 745

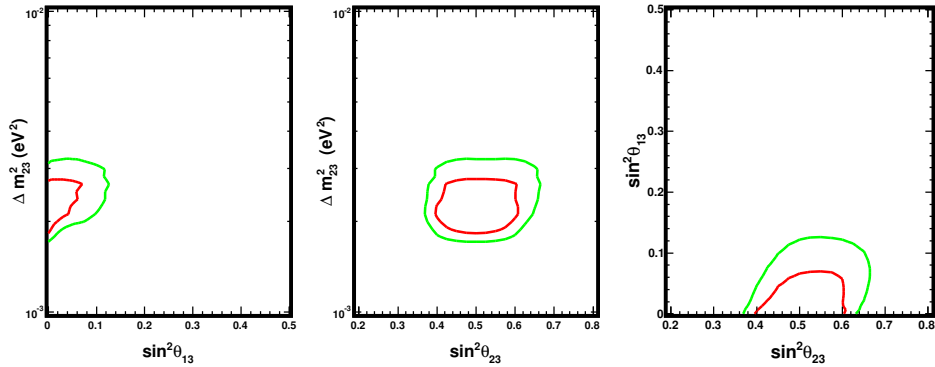


FIG. 4: Normal Hierarchy contours for SK-I + SK-II data set. The 90%(99%) allowed region appears in red (green).

latter provides the dominant constraint to the combined contour. Further, when these problematic bins are removed from the fit the size of the SK-II contour doubles in size, exceeding that of SK-I. Figures 7 and 8 show the zenith angle event distributions for SK-I and SK-II. Finally, to explore the effect of systematic biases in the selection of the e-like samples on the size of the contour, the data were re-fit with the associated systematic errors at double their nominal value and no appreciable change was found.

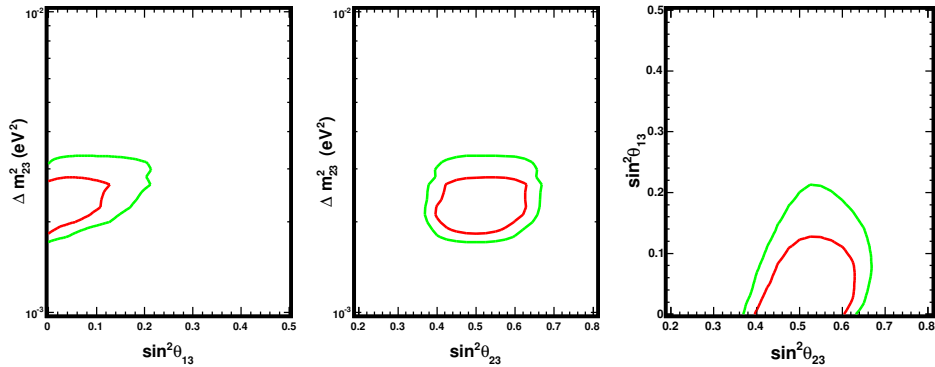


FIG. 5: Inverted hierarchy contours for SK-I + SK-II data set. The 90%(99%) allowed region appears in red (green)

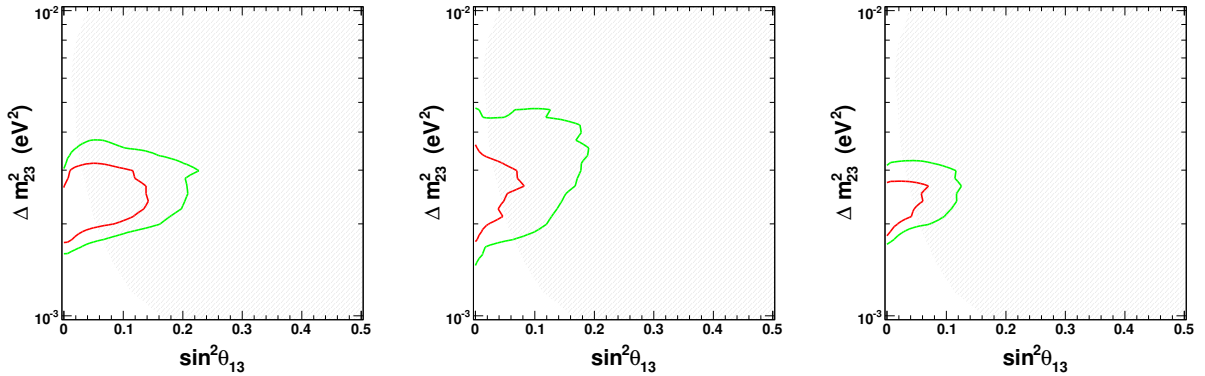


FIG. 6: CHOOZ exclusion contour at 90% overlaid with the allowed regions from the search for θ_{13} at 90% (99%) C.L. in red (green). From left to right the contours represent the results of the fits to the SK-I data alone, the SK-II data alone and the their combination.

B. Search for non-maximal θ_{23}

For the analysis of searching non-maximal θ_{23} , the constraint of $\sin^2\theta_{23}$ in scanning parameters of Δm_{23}^2 and $\sin^2\theta_{23}$ with assuming $\theta_{13} = 0$ is compared with one of $\sin^2\theta_{23}$ in the four dimensional oscillation parameter space including solar terms ($\Delta m_{12}^2, \sin^2\theta_{12}$).

In the case of the analysis including solar neutrino parameters (solar-on case), the scanning points of solar parameters are chosen around the allowed region obtained by a combined analysis of the solar neutrino data and KamLAND data [23] as shown as Figure 9.

To take into account the constraint on the solar neutrino parameters, the $\Delta\chi^2_{solar}$ value from the combined analysis of the solar neutrino and KamLAND data is added to $\Delta\chi^2$ from the atmospheric neutrino data for each ($\Delta m_{12}^2, \sin^2\theta_{12}$) scanning point.

Figure 11 shows the $\Delta\chi^2$ distributions with and without the solar parameters as function of $\sin^2\theta_{23}$, where $\Delta m_{12}^2, \Delta m_{23}^2$ and $\sin^2\theta_{12}$ are chosen so that χ^2 is minimized. the best-fit point without the solar parameters is located at $\sin^2\theta_{23} = 0.50$, on the other hand, the best-fit point with the solar terms is 0.49. The minimum χ^2 value is 832.5/748 d.o.f in case with the 1-2 parameters at ($\sin^2\theta_{23}, \Delta m_{23}^2, \sin^2\theta_{12}, \Delta m_{12}^2$) = (0.49, $2.09^{-3}eV^2$, 0.30, $7.59^{-5}eV^2$).

The gray scale in Figure 10 shows the $\chi^2 - \chi^2_{min}$ distribution at each solar parameter point. Since the difference of $\chi^2 - \chi^2_{min}$ in a 1-2 parameter plane is small (≤ 0.14), the global χ^2 distribution has weak dependence on the details for the 1-2 parameters.

Zenith angle dependence of the ratio between the number of FC Sub-GeV single-ring μ -like 1μ edecay events and FC Sub-GeV single-ring e-like 0μ edecay events for the data and the best-fit results with and without the solar terms are shown in Figure 12. The effect of the solar terms on the (N_μ/N_e) ratio has not been seen.

There is no significant discrepancy of $\sin^2\theta_{23}$ from 45° , but the asymmetric shape due to the effect of the solar terms is seen in the χ^2 distribution.

V. CONCLUSION

A three flavor oscillation fit to the first and second generation data of the Super-K data. No evidence for non-zero θ_{13} is found, and the best fit oscillation parameters in either hierarchy are $\Delta m^2 = 2.1 \times 10^{-3}eV^2$, $\sin^2\theta_{13} = 0.0$ and $\sin^2\theta_{23} = 0.5$. The value of θ_{13} is constrained to $\sin^2\theta_{13} < 0.07(0.13)$ in the normal (inverted) hierarchy at the 90% confidence level and is dominated by a downward fluctuation in a few bins of the SK-II Multi-GeV e-like sample. All fits are consistent with the CHOOZ experiment's upper limit and no preference for either mass hierarchy exists in the data. The search for non-maximal atmospheric mixing finds no evidence for a preferred octant for θ_{23} . However, the mixing angle is constrained at 1-sigma C.L. to $0.43 \leq \sin^2\theta_{23} \leq 0.55$.



FIG. 7: SK-I zenith angle distributions for the search for θ_{13} . Blue is MC at best fit. Red is at best fit with $\theta_{13} = \text{CHOOZ}$.

VI. ACKNOWLEDGMENTS

We gratefully acknowledge the cooperation of the Kamioka Mining and Smelting Company. The Super-Kamiokande experiment has been built and operated from funding by the Japanese Ministry of Education, Culture, Sports, Science and Technology, the United States Department of Energy, and the U.S. National Science Foundation. Some of us have been supported by funds from the Korean Research Foundation ,(BK21) and the Korea Science and Engineering Foundation.

-
- [1] T. Araki et al., Phys. Rev. Lett. **94**, 081801 (2005).
 - [2] J. Hosaka et al. (Super-Kamiokande), Phys. Rev. **D74**, 032002 (2006), hep-ex/0604011.
 - [3] J. Hosaka et al. (Super-Kamiokande), Phys. Rev. **D73**, 112001 (2006), hep-ex/0508053.
 - [4] Y. Ashie et al. (Super-Kamiokande), Phys. Rev. **D71**, 112005 (2005), hep-ex/0501064.

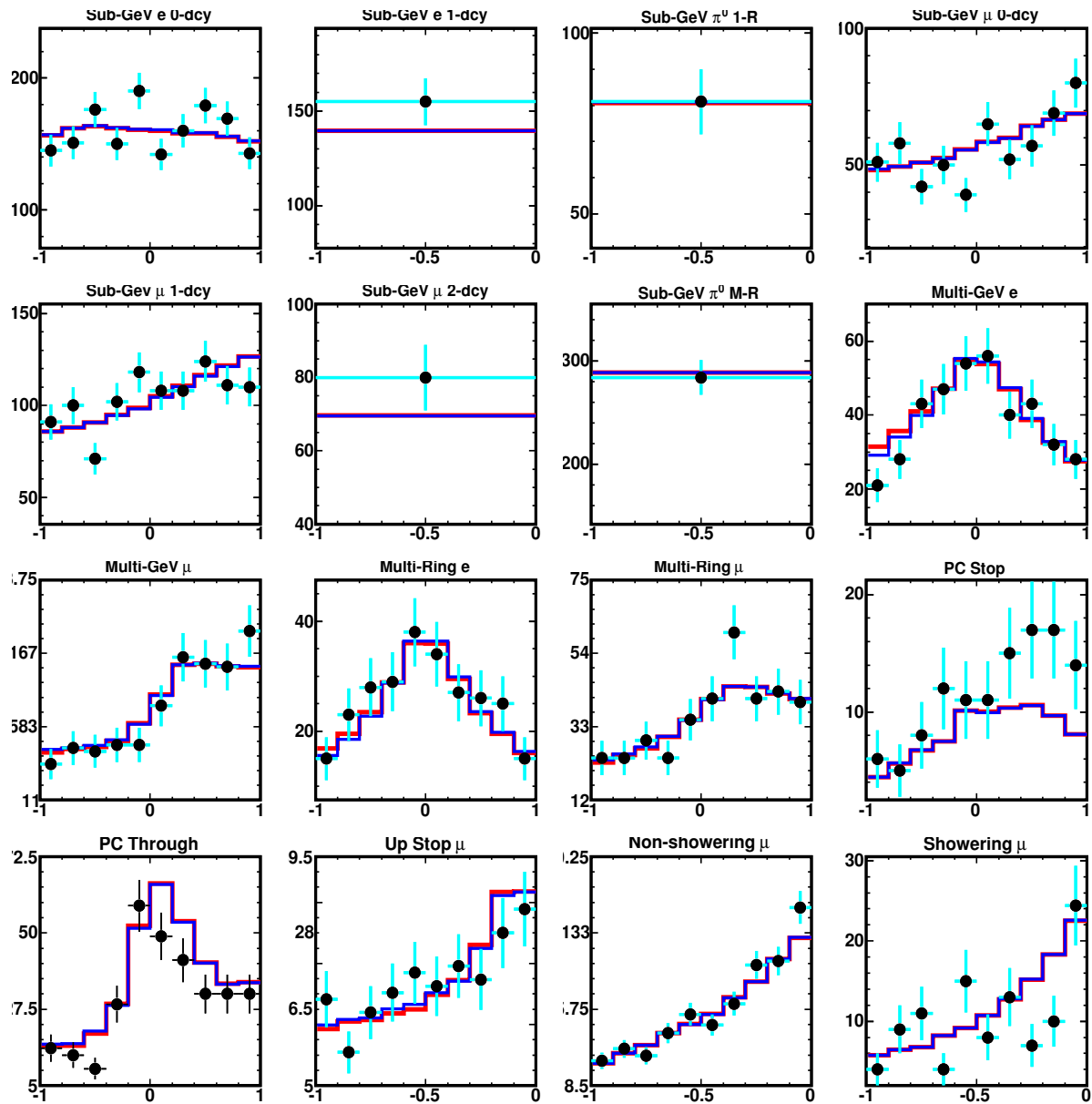


FIG. 8: SK-II zenith angle distributions for the search for θ_{13} . Blue is MC at best fit. Red is at best fit with $\theta_{13} = \text{CHOOZ}$. A deficit in the upward-going bins of the multi-GeV e-like sample and excess in the $\cos\Theta_z = -0.6$ bin of upward stopping muon sample that constrain the SK-II θ_{13} allowed region are shown.

- [5] B. Aharmim et al., Phys. Rev. **C72**, 055502 (2005).
- [6] A. Aguilar-Arevalo et al., Phys. Rev. Lett. **98**, 231801 (2007).
- [7] M. Ahn et al., Phys. Rev. **D74**, 072003 (2006).
- [8] P. Anderson et al., Phys. Rev. Lett. **101**, 131802 (2008).
- [9] Y. Itow et al. (T2K) (2001), hep-ex/0106019.
- [10] F. Ardellier et al. (Double Chooz) (2006), hep-ex/060625.
- [11] T. D. B. Collaboration (Daya Bay) (2007), hep-ex/0701029.
- [12] M. Apollonio et al., Phys. Lett. **B 466** (1999).
- [13] D. M. V. Barger and K. Wisnant, Phys. Rev. **D65**, 073023 (2002).
- [14] O. L. G. Peres and A. Y. Smirnov, Phys. Rev. Lett. **B 456**, 204 (1999).
- [15] O. L. G. Peres and A. Y. Smirnov, Nucl. Phys. B **680**, 479 (2004).
- [16] C. K. C. Giunti and M. Monteno, Nucl. Phys. **b521**, 3 (1998).
- [17] V. Barger et al., Phys. Rev. **D22**, 2718 (1980).
- [18] A. Dziewonski and D. Anderson, Phys. Earth, Planet, Interiors **25**, 297 (1981).

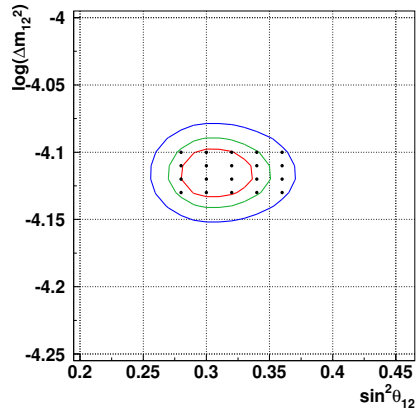


FIG. 9: The arrowed 1-2 parameters obtained from the results of the solar neutrino and KamLAND data [?]. The 20 points show the scanned points and the $\Delta\chi^2_{solar}$ from the solar plus KamLAND data at the each point is added to the χ^2 from the atmospheric neutrino data. Three contours correspond to the 68 % (dashed line), 90 % (solid line) and 99 % (dotted line).

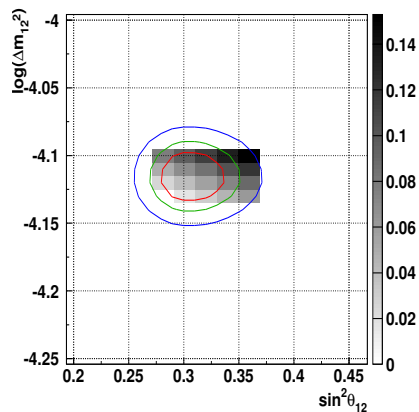


FIG. 10: $\chi^2 - \chi^2_{min}$ distribution as a function of Δm^2_{23} for oscillations without the 1-2 parameters (dashed line) and with the 1-2 parameters (solid line).

- [19] Y. Fukuda et al., Nucl. Instrum. Meth. **A501**, 418 (2003).
- [20] Y. Ashie et al. (Super-Kamiokande), Phys. Rev. Lett. **93**, 101801 (2004), hep-ex/0404034.
- [21] S. Desai et al., Astropart. Phys. **29**, 42 (2008).
- [22] G. Fogli et al., Phys. Rev. **D66**, 053010 (2002).
- [23] G. L. Fogli et al. (2008), hep-ph/0808.2016.

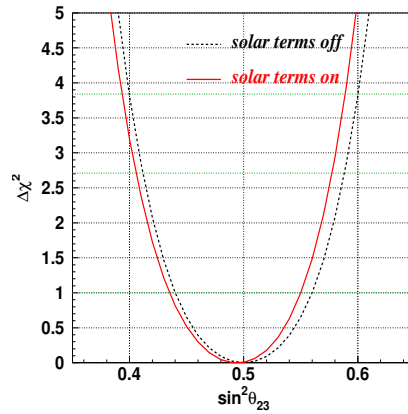


FIG. 11: $\chi^2 - \chi_{min}^2$ distribution as a function of $\sin^2\theta_{23}$ for oscillations without the 1-2 parameters (dotted line) and with the 1-2 parameters (solid line). For each $\sin^2\theta_{23}$ point, Δm_{23}^2 is chosen so that χ^2 is minimized. The green line corresponds to the 68% confidence level which is located at $\chi_{min}^2 + 1.0$.

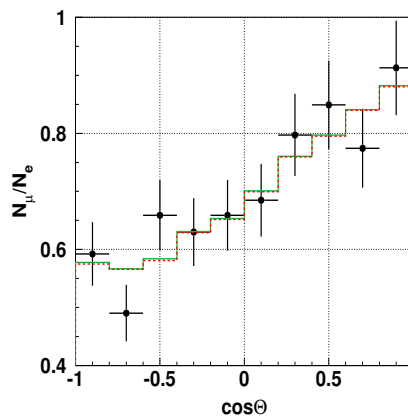


FIG. 12: Zenith angle dependence of (N_μ/N_e) for the data (dot), the best-fit results with solar terms (solid line) and the best-fit results without solar terms (dotted line). $N_\mu(N_e)$ is the number of events for FC Sub-GeV single-ring μ -like 1μ edecay sample (e-like 0μ edecay sample).